

Role of spin-orbit coupling in the Kugel-Khomskii model on the honeycomb lattice

Akihisa Koga, Shiryu Nakauchi, and Joji Nasu

Department of Physics, Tokyo Institute of Technology, Meguro, Tokyo 152-8551, Japan (Received 25 May 2017; revised manuscript received 29 January 2018; published 30 March 2018)

We study the effective spin-orbital model for honeycomb-layered transition metal compounds, applying the second-order perturbation theory to the three-orbital Hubbard model with the anisotropic hoppings. This model is reduced to the Kitaev model in the strong spin-orbit coupling limit. Combining the cluster mean-field approximations with the exact diagonalization, we treat the Kugel-Khomskii type superexchange interaction and spin-orbit coupling on an equal footing to discuss ground-state properties. We find that a zigzag ordered state is realized in the model within nearest-neighbor interactions. We clarify how the ordered state competes with the nonmagnetic state, which is adiabatically connected to the quantum spin liquid state realized in a strong spin-orbit coupling limit. Thermodynamic properties are also addressed. The present paper should provide another route to account for the Kitaev-based magnetic properties in candidate materials.

DOI: [10.1103/PhysRevB.97.094427](https://doi.org/10.1103/PhysRevB.97.094427)**I. INTRODUCTION**

Orbital degrees of freedom have been studied as a central topic of strongly correlated electron systems as they possess own quantum dynamics and are strongly entangled with other degrees of freedom such as charge and spin [1]. Recently, multi-orbital systems with strong spin-orbit coupling (SOC) have attracted considerable attention [2,3]. One of the intriguing examples is the series of the Mott insulators with honeycomb-based structures such as $A_2\text{IrO}_3$ ($A = \text{Na, Li}$) [4–6], and $\beta\text{-Li}_2\text{IrO}_3$ [7]. Due to a strong SOC for $5d$ electrons, the low-energy Kramers doublet, which is referred to as an isospin, plays an important role at low temperatures. Furthermore, anisotropic electronic clouds intrinsic in the t_{2g} orbitals result in peculiar exchange couplings between the isospins, which are suggested to be dominated by the Kitaev-type interaction [8,9]. The ground state of the pure Kitaev model is a quantum spin liquid (QSL), and hence a lot of experimental and theoretical works have been devoted to the iridium oxides in this context or to clarify the competition between the Kitaev model and other interactions yielding magnetic orders [10–18].

Very recently, the ruthenium compound $\alpha\text{-RuCl}_3$ with $4d$ electrons has been studied actively as another Kitaev candidate material [19–27]. In general, the SOC in $4d$ orbitals is weaker than that in $5d$ orbitals and is comparable with the exchange energy. Therefore, it is highly desired to deal with SOC and exchange couplings on an equal footing although the magnetic properties for honeycomb-layered compounds have been mainly discussed within the isospin model with the Kitaev and other exchange couplings including longer-range interactions [10,28–32].

In this paper, we study the role of the SOC in the Mott insulator with orbital degrees of freedom. We examine the localized spin-orbital model with the Kugel-Khomskii type superexchange interactions between nearest-neighbor sites [33] and onsite SOC on the two-dimensional honeycomb lattice. In the strong SOC limit, this model is reduced to the Kitaev model and the QSL state is realized. On the other hand, a conventional

spin-orbital ordered state may be stabilized in the small SOC case. To examine the competition between the magnetically disordered and ordered states in the intermediate SOC region, we first use the cluster mean-field (CMF) theory [34] with the exact diagonalization (ED). We determine the ground state phase diagram in the model and clarify that a zigzag magnetically ordered state is realized due to the competition between distinct exchanges. Calculating the specific heat and entropy in terms of the thermal pure quantum (TPQ) state [35], we discuss how thermodynamic properties characteristic of the Kitaev model appear in the intermediate SOC region.

The paper is organized as follows. In Sec. II, we introduce the three-orbital model and derive the effective Hamiltonian in the strong coupling limit. In Sec. III, we show the results for the ground state obtained by the CMF method to clarify the role of the SOC in the system. Thermodynamic properties are discussed in Sec. IV. A summary is provided in the last section.

II. EFFECTIVE HAMILTONIAN

We start with the three-orbital Hubbard model on the honeycomb lattice. This should be appropriate to describe the electronic state of the t_{2g} orbitals in the compounds $A_2\text{IrO}_3$ and $\alpha\text{-RuCl}_3$ since there exists a large crystalline electric field for the d orbitals. The transfer integral t between the t_{2g} orbitals via ligand p orbitals are evaluated from the Slater-Koster parameters, where the neighboring octahedra consisting of six ligands surrounding transition metal ions share their edges. Note that the transfer integrals involving one of the three t_{2g} orbitals vanish due to the anisotropic electronic clouds [9]. We refer to this as an inactive orbital and the other orbitals as active ones. These depend on three inequivalent bonds, which are schematically shown as the distinct colored lines in Fig. 1. Moreover, we consider the onsite intra- and interorbital Coulomb interactions, U and U' , Hund coupling K , and pair hopping K' in the conventional manner. In the following, we restrict our discussions to the conditions $U = U' + 2K$ and

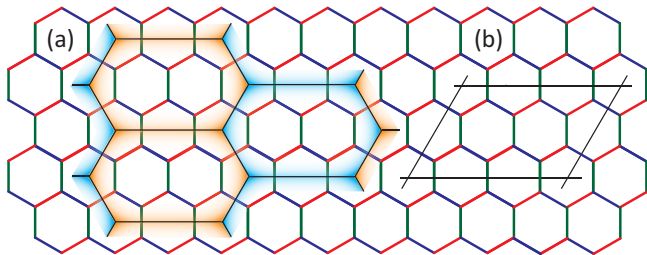


FIG. 1. Honeycomb lattice. Green, red, and blue lines denote x , y , and z bonds, respectively. (a) Two kinds of effective clusters with ten sites, which are colored in yellow and blue, are treated in the framework of the CMF method (see text). (b) Twelve-site cluster for the TPQ states.

$K' = K$, which are led by the symmetry argument of the degenerate orbitals.

We use the second-order perturbation theory in the strong coupling limit since the Mott insulating state is realized in the honeycomb-layered compounds. We then obtain the Kugel-Khomskii-type exchange model, assuming that five electrons occupy the t_{2g} orbitals in each site [36–39]. By taking the SOC into account, the effective Hamiltonian is explicitly given as

$$\mathcal{H} = \sum_{\langle ij \rangle_\gamma} \mathcal{H}_{ij}^{\text{ex}(\gamma)} - \lambda \sum_i \mathbf{L}_i \cdot \mathbf{S}_i, \quad (1)$$

where λ is the SOC, and \mathbf{S}_i and \mathbf{L}_i are spin and orbital angular-momentum operators at the i th site, respectively. The exchange Hamiltonian $\mathcal{H}_{ij}^{\text{ex}(\gamma)}$, which depends on the bond $\gamma (=x, y, z)$ of the honeycomb lattice (see Fig. 1), is given as $\mathcal{H}_{ij}^{\text{ex}(\gamma)} = \mathcal{H}_{1;ij}^{(\gamma)} + \mathcal{H}_{2;ij}^{(\gamma)} + \mathcal{H}_{3;ij}^{(\gamma)}$, with

$$\mathcal{H}_{1;ij}^{(\gamma)} = -2J_1 \left(\frac{3}{4} + \mathbf{S}_i \cdot \mathbf{S}_j \right) \left[-\tau_{ix}^{(\gamma)} \tau_{jx}^{(\gamma)} + \tau_{iy}^{(\gamma)} \tau_{jy}^{(\gamma)} + \tau_{iz}^{(\gamma)} \tau_{jz}^{(\gamma)} - \frac{1}{4} \tau_{i0}^{(\gamma)} \tau_{j0}^{(\gamma)} + \frac{1}{4} (\tau_{i0}^{(\gamma)} + \tau_{j0}^{(\gamma)}) \right], \quad (2)$$

$$\mathcal{H}_{2;ij}^{(\gamma)} = -2J_2 \left(\frac{1}{4} - \mathbf{S}_i \cdot \mathbf{S}_j \right) \left[\tau_{ix}^{(\gamma)} \tau_{jx}^{(\gamma)} - \tau_{iy}^{(\gamma)} \tau_{jy}^{(\gamma)} - \tau_{iz}^{(\gamma)} \tau_{jz}^{(\gamma)} + \frac{1}{4} \tau_{i0}^{(\gamma)} \tau_{j0}^{(\gamma)} + \frac{1}{4} (\tau_{i0}^{(\gamma)} + \tau_{j0}^{(\gamma)}) \right], \quad (3)$$

$$\mathcal{H}_{3;ij}^{(\gamma)} = -\frac{4}{3} (J_3 - J_2) \left(\frac{1}{4} - \mathbf{S}_i \cdot \mathbf{S}_j \right) \left[\tau_{ix}^{(\gamma)} \tau_{jx}^{(\gamma)} + \tau_{iy}^{(\gamma)} \tau_{jy}^{(\gamma)} - \tau_{iz}^{(\gamma)} \tau_{jz}^{(\gamma)} + \frac{1}{4} \tau_{i0}^{(\gamma)} \tau_{j0}^{(\gamma)} \right], \quad (4)$$

where we follow the notation of Ref. [36], and $J_1 = 2t^2/U[1 - 3K/U]^{-1}$, $J_2 = 2t^2/U[1 - K/U]^{-1}$, $J_3 = 2t^2/U[1 + 2K/U]^{-1}$ are the exchange couplings between nearest neighbor spins [36–39]. Here, we have newly introduced the orbital pseudospin operators $\tau_l^{(\gamma)}$ with $l = x, y, z, 0$. Note that its definition depends on the direction of the bond (γ bond) between the nearest neighbor pair $\langle ij \rangle$. $\tau_l^{(\gamma)}$ is represented by the 3×3 matrix based on the three orbitals: The 2×2 submatrix on the two active orbitals is given by $\sigma_l/2$ for $l = x, y, z$ and the identity matrix for $l = 0$, and the

other components for one inactive orbital are zero, where σ_l is the Pauli matrix. Now, we comment on the role of three kinds of spin-orbital Hamiltonians. Note that all eigenvalues of the orbital parts described in $[\dots]$ in Eqs. (2)–(4) are not negative. Thus, the Hamiltonian \mathcal{H}_1 enhances ferromagnetic correlations, while \mathcal{H}_2 and \mathcal{H}_3 lead to antiferromagnetic correlations. As for the orbital degrees of freedom, we find that both orbital parts of Eqs. (2) and (3) prefer the ferro-type orbital state. These should be understood by applying the Goodenough-Kanamori rule to our honeycomb system, where finite electron transfers between different orbitals via a 90-degree cation-anion-cation bridge favor ferromagnetic and ferro-orbital correlations. There exists orbital frustration due to the directional nature of the orbital degree of freedom [40] and competitions between these three interactions (J_1, J_2 , and J_3), which should stabilize nontrivial ground states. In the possible candidate phases, ferromagnetically ordered, zigzag, stripy, and Neel states, the number of nearest neighbor parallel bonds is 3, 2, 1, and 0, respectively. Therefore, one naively expects that the ferromagnetically and zigzag ordered states are the most appropriate candidates realized in the system.

What is most distinct from ordinary spin-orbital models is that the present system describes not only spin-orbital orders but also the QSL state realized in the Kitaev model. When the SOC is absent, the system is reduced to the standard Kugel-Khomskii type Hamiltonian. In the large Hund coupling case, the Hamiltonian $\mathcal{H}_{1;ij}^{(\gamma)}$ is dominant. Then, the ferromagnetically ordered ground state should be realized. In the smaller case of the Hund coupling, the ground state is not trivial due to the competing interactions, discussed above. On the other hand, in the case $\lambda \rightarrow \infty$, the SOC lifts the degeneracy in the t_{2g} orbitals at each site and the lowest Kramers doublet, $|\tilde{\sigma}\rangle = (|xy, \sigma\rangle \mp |yz, \bar{\sigma}\rangle + i|zx, \bar{\sigma}\rangle)/\sqrt{3}$, plays a crucial role for low temperature properties. Then, the model Hamiltonian Eq. (1) is reduced to the exactly solvable Kitaev model with the spin-1/2 isospin operator $\tilde{\mathbf{S}}$, as $\mathcal{H}_{\text{eff}} = -\tilde{J} \sum_{\langle ij \rangle_\gamma} \tilde{S}_{i\gamma} \tilde{S}_{j\gamma}$ ($\gamma = x, y, z$), where $\tilde{J} [=2(J_1 - J_2)/3]$ is the effective exchange coupling [8]. It is known that, in this effective spin model, the QSL ground state is realized with the spin gap. At finite temperatures, a fermionic fractionalization appears together with double peaks in the specific heat [15, 16]. In the following, we set the exchange coupling J_1 as a unit of energy. We then study ground-state and finite-temperature properties in the spin-orbital system with parameters K/U and λ/J_1 .

III. GROUND-STATE PROPERTIES

First, we discuss ground state properties in the spin-orbital model by means of the CMF method [34]. In the method, the original lattice model is mapped to an effective cluster model, where spin and orbital correlations in the cluster can be taken into account properly. Intercluster correlations are treated through several mean fields at i th site, $\langle S_{ik} \rangle, \langle \tau_{il}^{(\gamma)} \rangle$, and $\langle S_{ik} \tau_{il}^{(\gamma)} \rangle$, where $k = x, y, z$ and $l = x, y, z, 0$. These mean fields are determined via the self-consistent conditions imposed on the effective cluster problem. The method is comparable with the numerically exact methods if the cluster size is large and has successfully been applied to quantum spin [34, 41–43] and hard-core bosonic systems [44–46]. To describe some possible

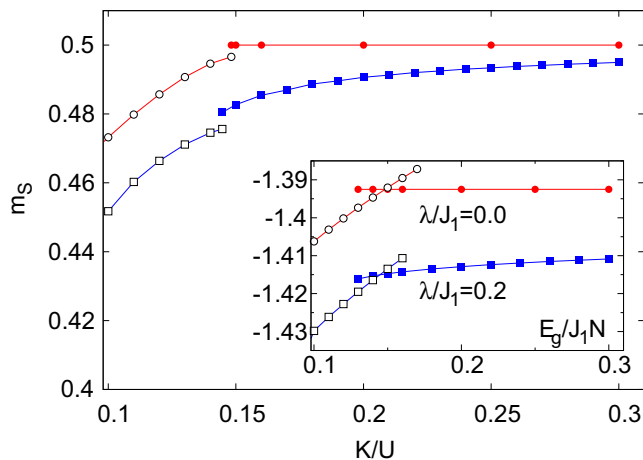


FIG. 2. The spin moments as a function of the Hund coupling K/U . Solid and open circles (squares) represent the results for the ferromagnetically and zigzag ordered states in the system with $\lambda/J_1 = 0.0$ (0.2). The ground state energy is shown in the inset.

ordered states such as the zigzag and stripy states [10], we introduce two kinds of clusters in the honeycomb lattice, which are shown as distinct colors in Fig. 1(a). Using the ED method, we self-consistently solve two effective cluster problems. Here, we will show the results for one of the mean-field solutions. To discuss magnetic properties at zero temperature, we calculate spin moment $m_S^\alpha = |\sum_i (-1)^{\delta_i^\alpha} \langle \mathbf{S}_i \rangle|/N$ and orbital angular momentum $m_L^\alpha = |\sum_i (-1)^{\delta_i^\alpha} \langle \mathbf{L}_i \rangle|/N$, where N is the number of sites and δ_i^α is the phase factor for an ordered state α .

We start with the system without SOC. Figure 2 shows the spin moments m_S^f and m_S^z for the ferromagnetically and zigzag ordered states, respectively, which are obtained by means of the ten-site CMF method (CMF-10). Namely, we have confirmed that other magnetically ordered states such as antiferromagnetic and stripy states are never stabilized in the present calculations, and thereby we do not show them in Fig. 2. With regard to the orbital state, we find that the realized magnetic orders are accompanied by the ferro-orbital order where the occupation rate in one (xy) orbital is larger than the others [see Figs. 3(c) and 3(d) at $K/U = 0.12$ and 0.3, respectively]. Meanwhile, the local angular momentum $\langle \mathbf{L}_i \rangle$ disappears in the case $\lambda = 0$. In the system with the large Hund coupling, the exchange coupling J_1 is dominant, and the ferromagnetically ordered ground state is realized with the fully-polarized moment $m_S^f = 0.5$, as shown in Fig. 2. On the other hand, in the smaller K region, the exchange couplings J_2 and J_3 are comparable with J_1 . Since \mathcal{H}_2 and \mathcal{H}_3 should enhance antiferromagnetic correlations, the ferromagnetically ordered state becomes unstable. We find that a zigzag magnetically ordered state is realized with finite m_S^z around $K/U \sim 0.12$. To study the competition between these ordered states, we show the ground state energies in the inset of Fig. 2. We clearly find the hysteresis in the curves, which indicates the existence of the first-order phase transition. By examining the crossing point, we clarify that the quantum phase transition between ferromagnetically and zigzag ordered states occurs at $K/U \sim 0.15$. In the case with $K/U < 0.1$, due to strong competitions, it is hard to obtain the converged

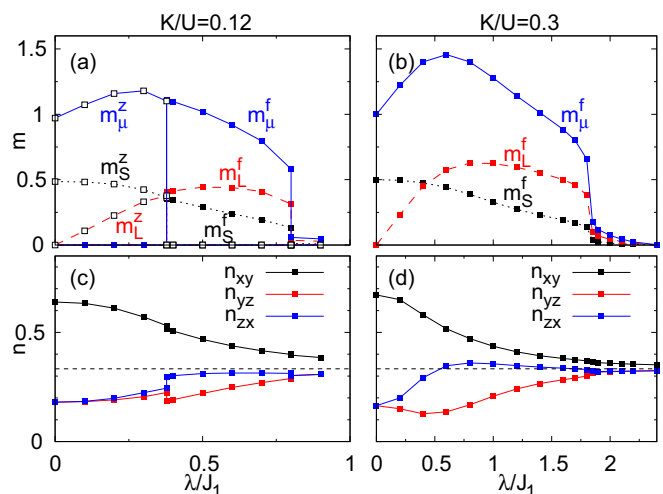


FIG. 3. Total magnetic moment m_μ , spin moment m_S , orbital moment m_L (upper panels), and the occupation rates of the t_{2g} orbitals (lower panels) in the spin-orbital systems with $K/U = 0.12$ (left panels) and $K/U = 0.3$ (right panels) as functions of the SOC.

solutions. This will be interesting to clarify this point in a future investigation.

The introduction of λ locally couples the spin and orbital degrees of freedom. The spin moments slightly decrease in both states, as shown in Fig. 2. The zigzag and ferromagnetically ordered states are stable against the small SOC, and the first-order transition point has little effect on the SOC. To discuss the stability of these states against the strong SOC, we calculate m_S and m_L in the system with $K/U = 0.12$ and 0.3, as shown in Fig. 3. The introduction of the SOC slightly decreases the spin moment, as discussed above. By contrast, the orbital angular momentum is induced parallel to the spin moment. Therefore, the total magnetic moment $m_\mu^\alpha = |\sum_i (-1)^{\delta_i^\alpha} \langle 2\mathbf{S}_i + \mathbf{L}_i \rangle|/N$ increases. When $K/U = 0.12$, the zigzag ordered state becomes unstable and the first-order phase transition occurs to the ferromagnetically ordered state at $\lambda/J_1 \sim 0.4$. Further increase of the SOC decreases the total moment m_μ^f . Finally, a jump singularity appears around $\lambda/J_1 \sim 0.8(1.8)$ in the system with $K/U = 0.12(0.3)$. It is also found that the magnetic moment is almost zero and each orbital is equally occupied as in the isospin states $|\bar{\sigma}\rangle$ in the larger SOC region as shown in Figs. 3(c) and 3(d). Therefore, we believe that this state is essentially the same as the QSL state realized in the Kitaev model.

By performing similar calculations, we obtain the ground state phase diagram, as shown in Fig. 4. The disordered (QSL) state is realized in the region with large λ/J_1 . The ferromagnetically ordered state is realized in the region with small λ/J_1 and large K/U . We wish to note that the zigzag ordered state is stable in the small SOC region, which is not directly taken into account in the Kitaev model. On the other hand, in the large λ case, the system is reduced to the Kitaev model. If one considers the classical limit of the model, the ground-state manifold includes the ferromagnetically ordered state but not the zigzag state. This should explain no direct phase transition between zigzag and QSL states, as shown in Fig. 4. In our calculations, the clusters are restricted to

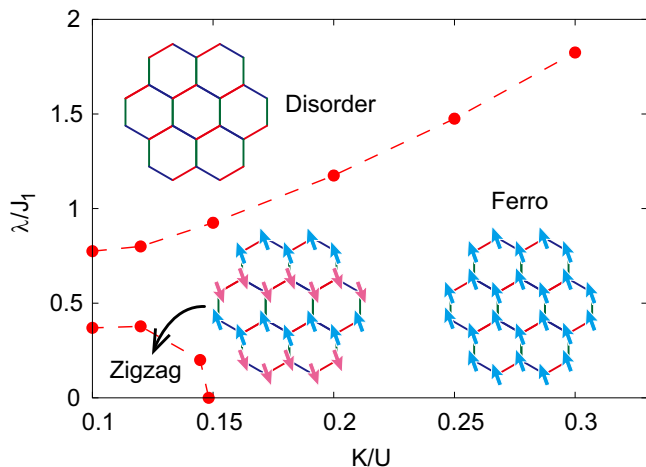


FIG. 4. The ground state phase diagram of the spin-orbital model. Transition points are obtained by the CMF-10. Spin configurations for disordered, zigzag ordered, and ferromagnetically ordered states are also shown.

be 10 sites, and we could not examine the cluster-size and shape dependence for the obtained results. Nevertheless, the numerical results are consistent with the above discussion, and therefore we believe that those capture the essence of the spin-orbital system on the honeycomb lattice.

IV. THERMODYNAMIC PROPERTIES

In this section we discuss thermodynamic properties in the system. It is known that, in the Kitaev limit ($\lambda \rightarrow \infty$), the excitations are characterized by two energy scales, which correspond to localized and itinerant Majorana fermions. This clearly appears in the specific heat as two peaks at $T/\tilde{J} = 0.012$ and 0.38 [16]. To clarify how the double peak structure appears in the intermediate SOC region, we make use of the TPQ state for the twelve-site cluster with the periodic boundary condition [see Fig. 1(b)]. According to the previous study [30], the double peak structure appears in the spin-1/2 Kitaev model even with the twelve-site cluster. Therefore, we believe that thermodynamic properties in the system can be discussed, at least, qualitatively in our calculations.

Here, we fix the Hund coupling as $K/U = 0.3$ to discuss finite temperature properties in the system with the intermediate SOC. Figure 5 shows the specific heat and entropy in the system with $\lambda/J_1 = 0, 1, 2, 4, \text{ and } 10$. In this calculation, the quantities are deduced by the statistical average of the results obtained from, at least, twenty independent TPQ states. When $\lambda = 0$, we find a broad peak around $T/J_1 = 0.4$ in the curve of the specific heat. In addition, with decreasing temperatures, most of the entropy is released at $T/J_1 \sim 0.1$, as shown in Fig. 5(b). This can be explained by the fact that ferromagnetic correlations are enhanced and spin degrees of freedom are almost frozen. The appearance of the large residual entropy should be an artifact in the small cluster with the orbital frustration.

The introduction of the SOC leads to interesting behavior. It is clearly found that the broad peak shifts to higher temperatures. This peak corresponds to the formation of the Kramers doublet, which is associated with the release of a part

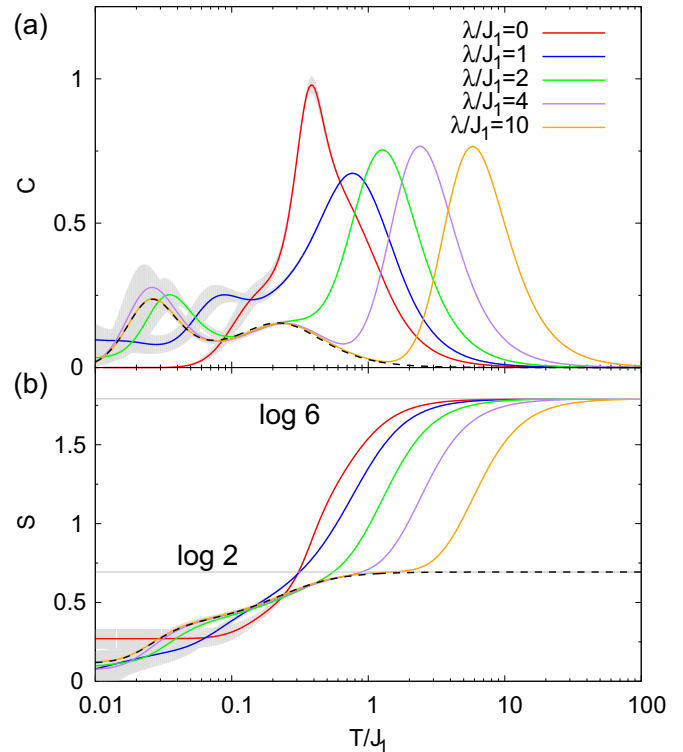


FIG. 5. The specific heat (a) and entropy (b) as a function of the temperature for the system with $\lambda/J_1 = 0, 1, 2, 4, \text{ and } 10$. Shaded areas are estimated by using the standard deviation of the results obtained from thirty initial random states. Dashed lines represent the results for the isospin Kitaev model with twelve sites.

of the entropy $\Delta S = \log(6) - \log(2)$ as shown in Fig. 5(b). Moreover, in the case $\lambda/J_1 \geq 2$, we find two peaks in the specific heat at lower temperatures almost independent of the SOC, and the curves are quantitatively consistent with the results for the isospin Kitaev model on the twelve sites, which are shown as dashed lines. Therefore, we believe that the Kitaev physics appears in the region. On the other hand, when $\lambda/J_1 = 1$, the specific heat exhibits a peak around $T/J_1 \sim 0.08$, indicating that the Kitaev physics is hidden by the formation of the Kramers doublet due to the competition between the exchange interaction and SOC.

IV. SUMMARY

We have studied the effective spin-orbital model obtained by the second-order perturbation theory. Combining the CMF theory with the ED method, we have treated the Kugel-Khomskii type superexchange interaction and SOC on an equal footing to determine the ground-state phase diagram. We have clarified how the magnetically ordered state competes with the nonmagnetic state, which is adiabatically connected to the QSL state realized in a strong SOC limit. Particularly, we have revealed that a zigzag ordered state is realized in this effective spin-orbital model with finite SOC. The present study suggests another mechanism to stabilize the zigzag ordered phase close to the QSL in the plausible situation

and also will stimulate further experimental studies in the viewpoint of the SOC effect on magnetic properties in Kitaev candidate materials. While we have considered only the SOC and superexchange interactions leading to the Kitaev model, it is also interesting to clarify the role of realistic parameters such as crystal-field splitting, direct hopping between d orbitals, and longer-range interaction. These are left for a future work.

ACKNOWLEDGMENTS

The authors would like to thank S. Suga for valuable discussions. Parts of the numerical calculations are performed in the supercomputing systems in ISSP, the University of Tokyo. This work was partly supported by the Grant-in-Aid for Scientific Research from JSPS, KAKENHI Grants No. JP17K05536, No. JP16H01066 (A.K.), No. JP16K17747, and No. JP16H00987 (J.N.).

-
- [1] Y. Tokura and N. Nagaosa, *Science* **288**, 462 (2000).
- [2] W. Witczak-Krempa, G. Chen, Y. B. Kim, and L. Balents, *Ann. Rev. Condens. Matter Phys.* **5**, 57 (2014).
- [3] H. Watanabe, T. Shirakawa, and S. Yunoki, *Phys. Rev. Lett.* **105**, 216410 (2010).
- [4] Y. Singh and P. Gegenwart, *Phys. Rev. B* **82**, 064412 (2010).
- [5] Y. Singh, S. Manni, J. Reuther, T. Berlijn, R. Thomale, W. Ku, S. Trebst, and P. Gegenwart, *Phys. Rev. Lett.* **108**, 127203 (2012).
- [6] R. Comin, G. Levy, B. Ludbrook, Z.-H. Zhu, C. N. Veenstra, J. A. Rosen, Y. Singh, P. Gegenwart, D. Stricker, J. N. Hancock, D. van der Marel, I. S. Elfimov, and A. Damascelli, *Phys. Rev. Lett.* **109**, 266406 (2012).
- [7] T. Takayama, A. Kato, R. Dinnebier, J. Nuss, H. Kono, L. S. I. Veiga, G. Fabbris, D. Haskel, and H. Takagi, *Phys. Rev. Lett.* **114**, 077202 (2015).
- [8] A. Kitaev, *Ann. Phys.* **321**, 2 (2006).
- [9] G. Jackeli and G. Khaliullin, *Phys. Rev. Lett.* **102**, 017205 (2009).
- [10] J. Chaloupka, G. Jackeli, and G. Khaliullin, *Phys. Rev. Lett.* **110**, 097204 (2013).
- [11] V. M. Katukuri, S. Nishimoto, V. Yushankhai, A. Stoyanova, H. Kandpal, S. Choi, R. Coldea, I. Rousochatzakis, L. Hozoi, and J. van den Brink, *New J. Phys.* **16**, 013056 (2014).
- [12] J. Knolle, D. L. Kovrizhin, J. T. Chalker, and R. Moessner, *Phys. Rev. Lett.* **112**, 207203 (2014).
- [13] Y. Yamaji, Y. Nomura, M. Kurita, R. Arita, and M. Imada, *Phys. Rev. Lett.* **113**, 107201 (2014).
- [14] J. Knolle, G.-W. Chern, D. L. Kovrizhin, R. Moessner, and N. B. Perkins, *Phys. Rev. Lett.* **113**, 187201 (2014).
- [15] J. Nasu, M. Udagawa, and Y. Motome, *Phys. Rev. Lett.* **113**, 197205 (2014).
- [16] J. Nasu, M. Udagawa, and Y. Motome, *Phys. Rev. B* **92**, 115122 (2015).
- [17] T. Suzuki, T. Yamada, Y. Yamaji, and S. I. Suga, *Phys. Rev. B* **92**, 184411 (2015).
- [18] J. Yoshitake, J. Nasu, and Y. Motome, *Phys. Rev. Lett.* **117**, 157203 (2016).
- [19] K. W. Plumb, J. P. Clancy, L. J. Sandilands, V. V. Shankar, Y. F. Hu, K. S. Burch, H.-Y. Kee, and Y.-J. Kim, *Phys. Rev. B* **90**, 041112 (2014).
- [20] Y. Kubota, H. Tanaka, T. Ono, Y. Narumi, and K. Kindo, *Phys. Rev. B* **91**, 094422 (2015).
- [21] J. A. Sears, M. Songvilay, K. W. Plumb, J. P. Clancy, Y. Qiu, Y. Zhao, D. Parshall, and Y.-J. Kim, *Phys. Rev. B* **91**, 144420 (2015).
- [22] M. Majumder, M. Schmidt, H. Rosner, A. A. Tsirlin, H. Yasuoka, and M. Baenitz, *Phys. Rev. B* **91**, 180401 (2015).
- [23] L. J. Sandilands, Y. Tian, K. W. Plumb, Y.-J. Kim, and K. S. Burch, *Phys. Rev. Lett.* **114**, 147201 (2015).
- [24] R. D. Johnson, S. C. Williams, A. A. Haghighirad, J. Singleton, V. Zapf, P. Manuel, I. I. Mazin, Y. Li, H. O. Jeschke, R. Valentí, and R. Coldea, *Phys. Rev. B* **92**, 235119 (2015).
- [25] J. Nasu, J. Knolle, D. L. Kovrizhin, Y. Motome, and R. Moessner, *Nat. Phys.* **12**, 912 (2016).
- [26] A. Koitzsch, C. Habenicht, E. Müller, M. Knupfer, B. Büchner, H. C. Kandpal, J. van den Brink, D. Nowak, A. Isaeva, and T. Doert, *Phys. Rev. Lett.* **117**, 126403 (2016).
- [27] L. J. Sandilands, Y. Tian, A. A. Reijnders, H.-S. Kim, K. W. Plumb, Y.-J. Kim, H.-Y. Kee, and K. S. Burch, *Phys. Rev. B* **93**, 075144 (2016).
- [28] H.-S. Kim, Vijay Shankar V., A. Catuneanu, and H.-Y. Kee, *Phys. Rev. B* **91**, 241110(R) (2015).
- [29] A. Banerjee, C. A. Bridges, J.-Q. Yan, A. A. Aczel, L. Li, M. B. Stone, G. E. Granroth, M. D. Lumsden, Y. Yiu, J. Knolle, S. Bhattacharjee, D. L. Kovrizhin, R. Moessner, D. A. Tennant, D. G. Mandrus, and S. E. Nagler, *Nat. Mater.* **15**, 733 (2016).
- [30] Y. Yamaji, T. Suzuki, T. Yamada, S. I. Suga, N. Kawashima, and M. Imada, *Phys. Rev. B* **93**, 174425 (2016).
- [31] S.-H. Do, S.-Y. Park, J. Yoshitake, J. Nasu, Y. Motome, Y. S. Kwon, D. T. Adroja, D. J. Voneshen, K. Kim, T.-H. Jang, J.-H. Park, K.-Y. Choi, and S. Ji, *Nat. Phys.* **13**, 1079 (2017).
- [32] S. M. Winter, K. Riedl, P. A. Maksimov, A. L. Chernyshev, A. Honecker, and R. Valentí, *Nat. Commun.* **8**, 1152 (2017).
- [33] K. I. Kugel and D. I. Khomskii, *Sov. Phys. Usp.* **25**, 231 (1982).
- [34] T. Oguchi, *Prog. Theor. Phys.* **13**, 148 (1955).
- [35] S. Sugiyra and A. Shimizu, *Phys. Rev. Lett.* **108**, 240401 (2012); **111**, 010401 (2013).
- [36] G. Khaliullin, *Prog. Theor. Phys.* **160**, 155 (2005).
- [37] B. Normand and A. M. Oleś, *Phys. Rev. B* **78**, 094427 (2008).
- [38] J. Chaloupka and A. M. Oleś, *Phys. Rev. B* **83**, 094406 (2011).
- [39] F. Trouselet, A. Ralko, and A. M. Oleś, *Phys. Rev. B* **86**, 014432 (2012).
- [40] D. I. Khomskii and M. V. Mostovoy, *J. Phys. A: Math. Gen.* **36**, 9197 (2003).
- [41] T. Sakai and M. Takahashi, *J. Phys. Soc. Jpn.* **58**, 3131 (1989).
- [42] A. Kawaguchi, A. Koga, K. Okunishi, and N. Kawakami, *Phys. Rev. B* **65**, 214405 (2002).
- [43] D. Yamamoto, *Phys. Rev. B* **79**, 144427 (2009).
- [44] S. R. Hassan, L. de Medici, and A.-M. S. Tremblay, *Phys. Rev. B* **76**, 144420 (2007).
- [45] D. Yamamoto, I. Danshita, and C. A. R. Sá de Melo, *Phys. Rev. A* **85**, 021601 (2012).
- [46] R. Suzuki and A. Koga, *JPS Conf. Proc.* **3**, 016005 (2014); *J. Phys. Soc. Jpn.* **83**, 064003 (2014).